Quantum dot microcavity control of photon statistics

Snijders, H.J.

Chapter 2

Semi-classical model for cavity QED

In this chapter, the interaction of a QD in a cavity with an incident light field is described from a semi-classical point of view. In the regime of low occupation number and weak optical driving, we find that the steady-state solution, in the linear regime, can also be derived from fully classical principles. Further, we give a simple extension of the semi-classical model for a two-level system in a cavity, in order to incorporate multiple polarized transitions, such as those appearing in neutral and charged quantum dots (QDs), and two nondegenerate linearly polarized cavity modes. Experimentally, we verify the model for a neutral QD in a micro-cavity and observe excellent agreement. The usefulness of this approach is demonstrated by investigating a single photon source based on polarization postselection, where we find an increase in the brightness for optimal polarization conditions predicted by the model.

Parts of this chapter are in preparation for publication.

2.1 Jaynes–Cummings model for continuous-wave laser light

A cavity quantum electrodynamics (CQED) system is, in its simplest form, a two-level system in a cavity which is driven by a light field. The interaction between photons and excitations of the two-level system is described by the so-called Jaynes–Cummings Hamiltonian interaction term $\hbar g\left(\hat{S}_{-}\hat{a}^{\dagger}+\hat{S}_{+}\hat{a}\right)$. This interaction term tells us that the creation of an excitation in the two-level system annihilates a photon in the cavity mode ($\hat{S}_{+}\hat{a}$) and vice versa. The strength of this interaction is given by the coupling constant g. A quantum description of a two-level system that interacts with a single optical cavity mode is described by the Jaynes–Cummings Hamiltonian ($\hbar = 1$) [15],

$$H_{jc} = \omega_c \hat{a}^{\dagger}\hat{a} + \omega_a \hat{S}_z + g\left(\hat{S}_{-}\hat{a}^{\dagger}+\hat{S}_{+}\hat{a}\right), \tag{2.1}$$

where ω_c is the cavity resonance frequency and ω_a is the transition frequency between the excited and ground-state energy levels. $\hat{a}^{\dagger}$ is the photon creation operator and $\hat{S}_{+}$ is the operator which creates an electron-hole pair in the QD and can be expressed by the familiar Pauli spin operators $\hat{S}_x$, $\hat{S}_y$, $\hat{S}_z$. Here, we define $\hat{S}_{+} = \frac{1}{2}|e\rangle\langle g| = \frac{1}{2}\left(\hat{S}_x + i\hat{S}_y\right)$, $\hat{S}_{-} = \frac{1}{2}|g\rangle\langle e| = \frac{1}{2}\left(\hat{S}_x - i\hat{S}_y\right)$ and $\hat{S}_z = \frac{1}{2}\left(|e\rangle\langle e| - |g\rangle\langle g|\right)$. These operators are related by the commutation relation $[\hat{S}_{-}, \hat{S}_{+}] = -2\hat{S}_z$.

It should be noted that the rotating wave approximation is used to obtain the Hamiltonian in Eq. 2.1. This means that the non-energy conserving terms are dropped, which are the terms that create or annihilate an excitation and a photon at the same time. Furthermore, we often drive the CQED system with an external light field. There are many light fields which can be considered, such as the classical fields of thermal light, coherent laser light, and pulsed laser light, or single-photon light as an example of a quantum light field. In this chapter, we focus only on continuous-wave coherent laser light, and in chapter 7, we discuss the case of pulsed laser light.

Now we describe the steady state solution of the light field in the cavity using a classical continuous-wave coherent laser coupled to a QD cavity system. Based on [16], an interaction term describing the interaction between the cavity field and an external laser is added to the Hamiltonian of Eq. 2.1, which becomes

$$H_1 = H_{jc} + H_D = \omega_c \hat{a}^{\dagger}\hat{a} + \omega_a \hat{S}_z + g\left(\hat{S}_{-}\hat{a}^{\dagger}+\hat{S}_{+}\hat{a}\right) + \eta\left(\hat{a}e^{i\omega_p t} + \hat{a}^{\dagger}e^{-i\omega_p t}\right). \tag{2.2}$$

In this equation, ω_p is the frequency of the laser which pumps the cavity field and η is the coupling rate between the optical amplitude of the laser and the cavity field. In general the coupling of a laser to the photons in the cavity is written as

$$C\left(\hat{a}\hat{a}_p^{\dagger}e^{i\omega_p t} + \hat{a}^{\dagger}\hat{a}_p e^{-i\omega_p t}\right), \tag{2.3}$$

where C is a coupling constant. For a classical field, $\hat{a}_p$ can be replaced by the field amplitude and as a result, Eq. 2.3 becomes

$$\approx \eta\left(\hat{a}e^{i\omega_p t} + \hat{a}^{\dagger}e^{-i\omega_p t}\right), \tag{2.4}$$

where $\hat{a}_p$ is absorbed in η. We can express the mean photon number in terms of η and the cavity loss rate κ,

$$\langle n\rangle = \left(\frac{\eta}{\kappa}\right)^2 = \frac{P_{\text{laser}}}{P_{\text{n=1}}}. \tag{2.5}$$

Here, P_{laser} is the laser power and $P_{\text{n=1}}$ is the laser power required to obtain $\langle n \rangle = 1$. If the cavity loss is purely linear, we can define $P_{\text{n=1}} \equiv \hbar\omega_a\kappa$, and one finds that η is related to the input power as

$$\eta = \sqrt{\left(P_{laser}\kappa\right) / \left(\hbar\omega_a\right)}. \tag{2.6}$$

Assuming a wavelength $\lambda = 930$ nm and a loss rate $\kappa = 10$ GHz, we find $P_{n=1} \approx 2\,\text{nW}$. Typically, we operate the system at a low driving power where the mean photon number $\langle n \rangle$ is between 0.01 and 0.001. This corresponds to a driving power between 1 and 10 pW.

In order to find the steady state solution of Eq. 2.2, the time-dependent part in the Hamiltonian should be removed. This is done by transforming the Hamiltonian to the Heisenberg picture with the unitary transformation

$$U(t) = \exp(-i\omega_p\hat{a}^\dagger\hat{a}t - i\omega_p\hat{S}_z t). \tag{2.7}$$

With this, the Hamiltonian becomes

$$H = U^\dagger H_1 U - iU^\dagger\frac{\partial}{\partial t}U = U^\dagger H_1 U - \omega_p\hat{a}^\dagger\hat{a} - \omega_p\hat{S}_z. \tag{2.8}$$

By inserting H_1 we obtain

$$H = (\omega_c - \omega_p)\hat{a}^\dagger\hat{a} + (\omega_a - \omega_p)\hat{S}_z + U^\dagger\left(g\left(\hat{S}_-\hat{a}^\dagger + \hat{S}_+\hat{a}\right) + \eta\left(\hat{a}e^{i\omega_p t} + \hat{a}^\dagger e^{-i\omega_p t}\right)\right)U. \tag{2.9}$$

In order to simplify this equation further, we make use of the Baker–Campbell–Hausdorff lemma and find

$$e^{i\omega_p t\hat{a}^\dagger\hat{a}}\hat{a}^\dagger e^{-i\omega_p t\hat{a}^\dagger\hat{a}} \approx \hat{a}^\dagger + \frac{\omega_p t}{1!}\left[\hat{a}^\dagger\hat{a}, \hat{a}^\dagger\right] + \frac{(\omega_p t)^2}{2!}\left[\hat{a}^\dagger\hat{a}, \left[\hat{a}^\dagger\hat{a}, \hat{a}^\dagger\right]\right] + ... \tag{2.10}$$

$$e^{i\omega_p t\hat{a}^\dagger\hat{a}}\hat{a}^\dagger e^{-i\omega_p t\hat{a}^\dagger\hat{a}} = \hat{a}^\dagger e^{i\omega_p t}. \tag{2.11}$$

Here we have used the bosonic commutation relation for photons

$$\left[\hat{a}^\dagger, \hat{a}\right] = 1. \tag{2.12}$$

Note that this nicely cancels out the time-dependent parts in Eq. 2.9. For the term $\hat{S}_+$, one finds in a similar manner $U^\dagger\hat{S}_+U = \hat{S}_+e^{i\omega_p t}$ by making use of the commutation relation

$$\left[\hat{S}_z, \hat{S}_+\right] = \hat{S}_+. \tag{2.13}$$

This results in the time-independent Hamiltonian

$$H = (\omega_c - \omega_p)\,\hat{a}^\dagger\hat{a} + (\omega_a - \omega_p)\,\hat{S}_z + g\left(\hat{S}_-\hat{a}^\dagger + \hat{S}_+\hat{a}\right) + \eta\left(\hat{a} + \hat{a}^\dagger\right). \tag{2.14}$$

Finally, we use the fact that the electron number is conserved and find that $\hat{S}_z = \frac{1}{2}\left(\hat{S}_+\hat{S}_- - \hat{S}_-\hat{S}_+\right) = \frac{1}{2}\left(|e\rangle\langle e| - |g\rangle\langle g|\right) = |e\rangle\langle e| - \frac{1}{2} = \hat{S}_+\hat{S}_- - \frac{1}{2}$. After dropping $-\frac{1}{2}$ vacuum energy we are left with

$$H = (\omega_c - \omega_p)\,\hat{a}^\dagger\hat{a} + (\omega_a - \omega_p)\,\hat{S}_+\hat{S}_- + g\left(\hat{S}_-\hat{a}^\dagger + \hat{S}_+\hat{a}\right) + \eta\left(\hat{a} + \hat{a}^\dagger\right). \tag{2.15}$$

Neglecting the zero-point energy for the free-field Hamiltonian and the QD Hamiltonian is allowed since it only gives a relative shift and does not affect the dynamics.

2.2 Semi-classical model in the linear regime

In the linear regime we assume that the incoming field is very weak, and as a result, the QD population remains approximately in the ground state $|g\rangle$, or in other words $\left\langle \hat{S}_z \right\rangle \approx -\frac{1}{2}$. In addition to the coherent dynamics described by Eq. 2.15, there are two dissipative channels in the system: the QD may spontaneously emit into modes other than the preferred cavity mode at a rate $\gamma_{||}$, and photons may pass through a cavity mirror at a rate κ. We neglect here non-radiative decay and pure dephasing. The master equation describing the driven damped evolution [17] is

$$\begin{gathered}\hat{H} = (\omega_c - \omega_p)\hat{a}^\dagger\hat{a} + (\omega_a - \omega_p)\hat{S}_+\hat{S}_- + g(\hat{S}_-\hat{a}^\dagger + \hat{S}_+\hat{a}) + \eta(\hat{a} + \hat{a}^\dagger) \\ \frac{d\rho}{dt} = \mathfrak{L}\rho = -i\left[\hat{H}, \rho\right] + 2\kappa\mathfrak{D}\left[\hat{a}\right]\rho + \gamma_{||}\mathfrak{D}\left[\hat{S}_-\right]\rho,\end{gathered} \tag{2.16}$$

where ρ is the density matrix of the QD-cavity system, $\mathfrak{L}$ is the Liouvillian superoperator and $\mathfrak{D}\left[\hat{a}\right]\rho = \frac{1}{2}\left(2\hat{a}\rho\hat{a}^\dagger - \hat{a}^\dagger\hat{a}\rho - \rho\hat{a}^\dagger\hat{a}\right)$ is a Lindblad type of dissipation. Note the factor of two difference between κ and $\gamma_{||}$, this is because there are two cavity mirrors. There are two approaches to obtain an analytical solution. In the first approach, we write down the equations of motion for the Heisenberg operators using Eq. 2.16. Using this approach, the mean value of the operator $O = \left\{\hat{a}, \hat{S}_-\right\}$ is given by $\left\langle \dot{O} \right\rangle = Tr\left(O\dot{\rho}\right)$, which leads to

$$\begin{gathered}\langle\dot{a}\rangle = -\kappa(1 - i\Delta_c)\langle\hat{a}\rangle + ig\left\langle \hat{S}_- \right\rangle + i\eta \\ \left\langle \dot{S}_- \right\rangle = -\gamma_\perp(1 - i\Delta_Q)\left\langle \hat{S}_- \right\rangle - i2g\left\langle \hat{a}\hat{S}_z \right\rangle \approx -\gamma_\perp(1 - i\Delta_Q)\left\langle \hat{S}_- \right\rangle + ig\langle\hat{a}\rangle,\end{gathered} \tag{2.17}$$

where $\Delta_c = (\omega_p - \omega_c)/\kappa$ is the normalized cavity-laser detuning, $\Delta_Q = (\omega_p - \omega_a)/\gamma_\perp$ is the normalized QD-laser detuning and $\gamma_\perp = \frac{\gamma_{||}}{2}$. Here we assume that $\left\langle \hat{S}_z \right\rangle \approx -\frac{1}{2}$ and that one can factorize the operator products. For clarity, we have removed the "hat" for $\langle\dot{a}\rangle$ and $\left\langle \dot{S}_- \right\rangle$.

In the second approach, we write the Hamiltonian in Eq. 2.2 as an effective Hamiltonian $H_{eff} = H - i\kappa\hat{a}^\dagger\hat{a} - i\gamma_\perp\hat{S}_+\hat{S}_-$ [18]. The equations of motion for the operators $\hat{a}$ and $\hat{S}_-$ can now be derived from the modified Heisenberg equations, $\frac{d\hat{S}_-}{dt} = i\left[H_{eff}, \hat{S}_-\right]$ and $\frac{d\hat{a}}{dt} = i\left[H_{eff}, \hat{a}\right]$, which results in the same set of equations as given in 2.17. In the weak excitation limit, the steady-state solution for the amplitude of the field in the cavity is given as

$$\langle\hat{a}\rangle = \frac{i\eta}{\kappa\left(1 - i\Delta_c\right) + \frac{g^2}{\gamma_\perp\left(1 - i\Delta_Q\right)}}. \tag{2.18}$$

Rewriting this equation in the form of an amplitude transmission coefficient for a single mode electric field gives

$$E = \eta_{out} \frac{1}{1 - i\Delta_c + \frac{C}{1 - i\Delta_Q}}, \tag{2.19}$$

where $\eta_{out} = i\eta/\kappa$ and $C = g^2/\kappa\gamma_\perp$. Here, C is the cooperativity, which is a measure of the interaction strength between the QD and cavity. In literature, the value $1/C$ is often defined as the "critical atom number", which roughly describes the number of atoms (or QDs) needed to drastically change the properties of the system. Remember that κ is defined as the loss rate of a single mirror; for the total loss rate of both mirrors we find $\kappa_{tot} = 2\kappa$. Similar to a micropillar cavity with a single input and a single output channel, one can also find the output field for a cavity coupled to two or more waveguides [19].

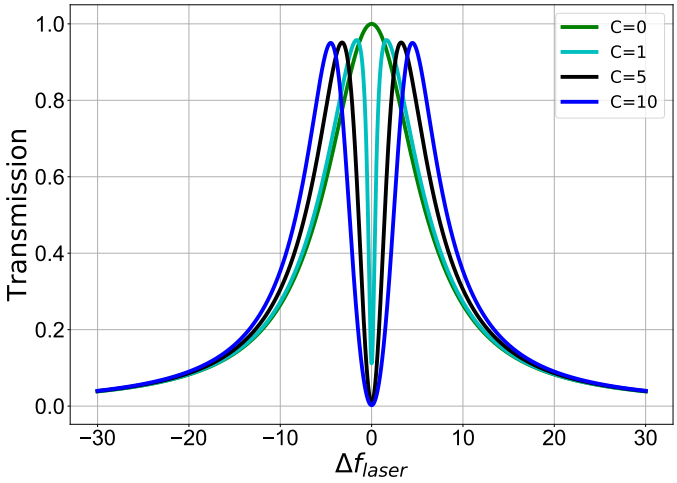

Figure 2.1: Transmission of the cavity field amplitude in Eq. 2.19 as a function of the laser detuning. Parameters: $\eta_{out} = 1$, $\kappa = 12$ GHz and $\gamma = \frac{1}{2\pi}$ GHz.

In Fig. 2.1 the normalized transmission is plotted as a function of the laser detuning for different values of the cooperativity C. By increasing C, the QD resonance dips become deeper and wider. In this thesis we work with QD-cavity systems which have a cooperativity of $C \sim 1$.

Additionally, it is possible to take saturation effects into account by assuming that the QD population does not remain in the ground state [20]. We call this regime the non-linear regime. In this case the QD transmission dip, shown for different cooperativity in Fig. 2.1, saturates at higher input powers, while for low powers the theory reduces to Eq. 2.19. In section 2.7 this is mathematically worked out and discussed in more detail.

2.3 Classical derivation of the semi-classical model

Here, we derive Eq. 2.19 from fully classical principles, and without using the Bloch equations. We consider two equal mirrors with reflection coefficient r and transmission coefficient t at a distance L, like a Fabry-Pérot resonator. The round-trip phase ϕ_0 in the electric field propagation term, written in terms of the wavelength λ_0, refractive index n and length L of the cavity, is:

$$\phi_0 = \frac{2\pi}{\lambda_0} n\,(2L) = \frac{4\pi n L}{c} f, \tag{2.20}$$

where c is the speed of light and f the frequency of the laser. Since the laser frequency will be scanned across the resonance frequency f_c of the Fabry-Pérot cavity, it is convenient to write the phase shift in terms of the relative frequency:

$$\phi = \frac{4\pi n L}{c}\,(f - f_c)\,. \tag{2.21}$$

Further, we assume that there is dispersion and loss in the cavity. We quantify loss of the cavity by single pass amplitude loss a_0. The QD transition is described by a harmonic oscillator. In the rotating wave approximation, a driven damped harmonic oscillator has a frequency-dependent response similar to a complex Lorentzian. Including cavity loss, QD loss a_{QD} and dispersion, we obtain a phase change in half a round trip of

$$\exp\left(-a + i\frac{\phi}{2}\right), \quad \text{where } a \equiv a_0 + \frac{a_{QD}}{1 - i\Delta'}. \tag{2.22}$$

Here, $\Delta' = (f - f_{QD})/\gamma_\perp$ with the resonance frequency of the QD f_{QD}. By summing over all possible round trips, the total transmission amplitude is

$$t_{tot} = tt \exp(-a + i\phi/2)\left[\sum_{n=0}^{\infty} \left(r^2 \exp(-2a + i\phi)\right)^n\right] \tag{2.23}$$

which becomes

$$t_{tot} = \frac{t^2 \exp(-a + i\phi/2)}{1 - r^2 \exp(-2a + i\phi)}. \tag{2.24}$$

This formula can be written in a form similar to the semi-classical model by considering $R \sim 1$, small phase changes in the cavity $\phi \ll 1$, in combination with $a_{QD} \ll 1$. This allows us to use a Taylor expansion of the exponentials in Eq. (2.24). By including all first-order contributions and a few second-order contributions, we write the complex transmission amplitude as

$$t_{tot} \approx \eta_{out} \frac{1}{1 - 2i\Delta + \frac{2C}{1 - i\Delta'}}, \tag{2.25}$$

with the out-coupling efficiency

$$\eta_{out} = \frac{1}{\sqrt{1 + 2a_0\left(\frac{1+R}{1-R}\right)}}. \tag{2.26}$$

In section 2.7 we show how to derive Eq. (2.25) and explain that the higher order Taylor contributions, which are added to be able to write the final formula in a compact form, are negligible. The out-coupling efficiency η_{out} gives the probability that a photon leaves the cavity through one of the mirrors. In Eq. (2.25), Δ is the normalized laser-cavity detuning and Δ' is the normalized detuning with respect to the QD transition. Here, f, f_c, and f_{QD} are the frequencies for the laser, cavity and QD, respectively. The result of Eq. (2.25) is equal to the result of the optical Bloch equations and shows that, using a fully classical model, it is possible to derive Eq. (2.25).

2.4 Polarization effects and multiple transitions in the semi-classical model

Understanding the interaction of a two-level system, such as atomic transitions or excitonic transitions in a semiconductor quantum dot (QD), with an optical cavity mode, is key for designing efficient single photon sources [2, 3], quantum photonic logic gates [21] and quantum networks [22]. Traditionally, the interaction of a two-level quantum system with an electromagnetic mode is described by the optical Bloch equations. There are two approaches to use the Bloch equations in describing such a cavity-QED system: a full quantum treatment where next to the QD also the light field is quantized [23] or a semi-classical approach where the light field is treated classically and atom-field correlations are neglected. This last approach leads to a well known analytical expression for the transmission of an emitter in a cavity [24, 19] for the weak and strong coupling regimes [25].

We focus here on QD-cavity systems in the weak coupling regime ($g \ll \kappa$). In this case, the transmission amplitude of the system is given by the, in section 2.2 derived, semi-classical model [19, 24, 17, 26]

$$t \approx \eta_{out} \frac{1}{1 - 2i\Delta + \frac{2C}{1-i\Delta'}}, \tag{2.27}$$

where η_{out} is the out-coupling efficiency and gives the probability amplitude that a photon leaves the cavity through one of the mirrors (we assume two identical mirrors). In Eq. (2.27), $\Delta = (f - f_c)/\kappa$ is the normalized detuning of the laser frequency f with respect to the cavity resonance frequency f_c (with cavity loss rate κ), and $\Delta' = \left(f - f^{'}\right)/\gamma_{\perp}$ is the normalized detuning with respect to the QD resonance $f^{'}$ (with dephasing rate $\gamma_{\perp} = \frac{\gamma_{||}}{2} + \gamma^*$). Δ is related to the round trip phase by $\varphi \approx \Delta \frac{\pi}{\mathcal{F}}$, where $\mathcal{F}$ is the finesse of the cavity. The coupling of the QD to the cavity mode is given by the cooperativity parameter $C = \frac{g^2}{\kappa\gamma_{\perp}}$ where g is the QD-cavity coupling strength.

In the Section 2.3 we have shown how Eq. (2.27) can be derived in a fully classical way by considering a QD in a Fabry-Pérot type optical resonator. In order to arrive at this result we consider that the laser is close to the cavity resonance, such that the phase changes are small and can be approximated by a leading-order Taylor expansion. Additionally, the two-level system is approximated by a driven damped harmonic oscillator. Here, we focus on QD-cavity systems but our results are valid for a large range of cavity QED systems.

The goal of this section is to show how Eq. (2.27) can be extended to a more general form

by considering two polarization-split (fundamental) optical cavity modes, a certain input and output polarization, and multiple optical QD transitions. This extension is important because it is experimentally difficult to produce perfectly polarization degenerate microcavities [27, 28], and the non-polarization degenerate case has attracted attention recently [29, 30]. An additional complication is that, instead of a two-level system, one often deals with V-level (fine-structure-split neutral exciton transitions) or 4-level (charged exciton transitions) systems [31]. The model presented here does not take into account the population of the excited state and non-resonant emission, including phonon-assisted transitions and spin flips. Finally, we compare our model to experimental data and demonstrate that it can be used to significantly increase the brightness of a single-photon source.

In Fig. 2.2, we show a sketch of a polarized QD-cavity system with two cavity modes (H,V) and two QD transitions (X,Y). For the specific case of linearly polarized input light ($\theta_{in} = 45°$), we plot the transmission as a function of the laser frequency in the inset of Fig. 2.2. The system is described as a cavity with polarization birefringence but without dichroism, under the reasonable assumption that losses in the cavity are polarization-independent. We use a Jones formalism in the polarization basis of the cavity, where the normalized detuning Δ from Eq. (2.27) becomes the matrix:

$$\begin{pmatrix} 2i\Delta_H & 0 \\ 0 & 2i\Delta_V \end{pmatrix}. \tag{2.28}$$

Drawing a parallel with the semi-classical model of a single cavity mode with a single QD transition allows us to split the contributions for a single round trip into a part due to the empty cavity and a part given by the QD interaction. The interaction with the QD modifies the round-trip phase and is given by the transmission matrix X (see table 2.1). This matrix is diagonal in the basis of the QD eigenpolarizations and has to be rotated into the polarization basis of the cavity by $R_{-\theta_{QD}} X R_{\theta_{QD}}$ with

$$R_{\theta_{QD}} = \begin{pmatrix} \cos\theta_{QD} & -\sin\theta_{QD} \\ \sin\theta_{QD} & \cos\theta_{QD} \end{pmatrix}. \tag{2.29}$$

Here, θ_{QD} is the angle between the cavity and QD polarization axis (see Fig. 2.2). The matrix X is constructed by adding up the QD transitions, taking care of their (magnetic-field dependent) polarization by the appropriate Jones matrix [32] and the Lorentzian frequency-dependent phase shift

$$\varphi_i = \frac{2C_i}{1 - i\Delta_i^{'}}, \tag{2.30}$$

where $\Delta_i^{'} = \left(f - f_i^{'}\right)/\gamma_{\perp i}$ is the normalized frequency detuning and C_i the coupling strength. The resonance frequencies $f_i^{'}$ are the eigenvalue of the QD Hamiltonian including electron-hole exchange and Zeeman interaction [33]. In table 2.1, X is given for neutral and charged QDs for different magnetic field configurations.

By adding all contributions, as one would do in a non-birefringent Fabry-Pérot cavity without QD [34], we find that the tiny changes after each round trip add up to a sizable effect after many round trips. From Eq. (2.25), we observe that the transmission for a single round trip can be written as

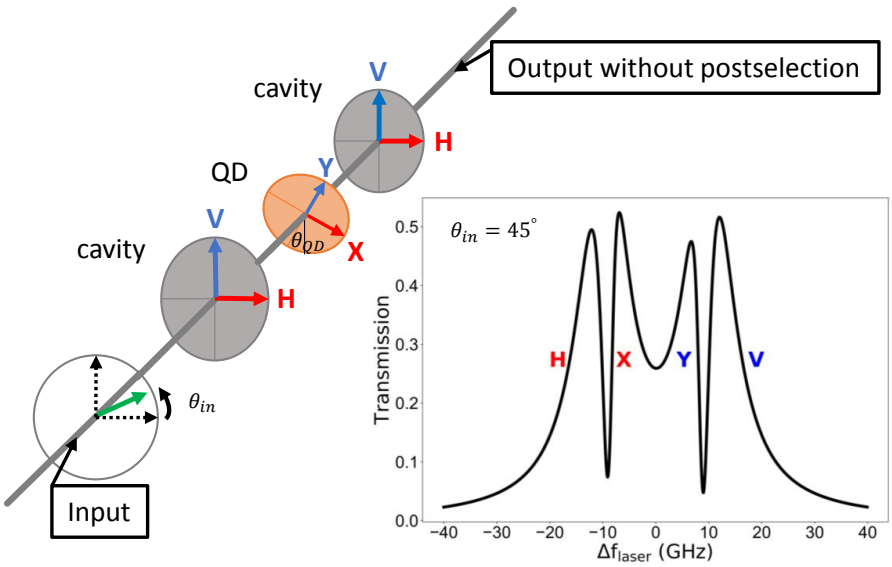

Figure 2.2: Sketch of a polarized cavity–neutral QD system. H and V denote the linearly polarized cavity modes and X and Y represent the polarization axes of the QD at an angle θ_{QD} with respect to the H cavity polarization. In this particular case the incident light is linearly polarized but in general an arbitrary polarization can be chosen. The inset shows the transmission spectrum for linear polarized light at an angle $\theta_{in} = 45°$. The difference in dip depth between the X and Y transition is due to the angle θ_{QD}. Here, no polarization postselection is done. Parameters are $f_H = -10\,\mathrm{GHz}$, $f_V = 10\,\mathrm{GHz}$, $f_X^{'} = -9\,\mathrm{GHz}$, $f_Y^{'} = 9\,\mathrm{GHz}$, $\theta_{QD} = 10°$.

B-field configuration	neutral QD	singly charged QD
No B-field	$\varphi_H(\omega_l)\boldsymbol{H} + \varphi_V(\omega_l)\boldsymbol{V}$	$\varphi_I(\omega_l)\boldsymbol{I}$
B, Faraday	$\varphi_R(\omega_l)\boldsymbol{R} + \varphi_L(\omega_l)\boldsymbol{L}$ (for large B)	$\varphi_R(\omega_l)\boldsymbol{R} + \varphi_L(\omega_l)\boldsymbol{L}$
B, Voigt	$[\varphi_1(\omega_l) + \varphi_3(\omega_l)]\,\boldsymbol{H} + [\varphi_2(\omega_l) + \varphi_4(\omega_l)]\,\boldsymbol{V}$	$[\varphi_1(\omega_l) + \varphi_3(\omega_l)]\,\boldsymbol{H} + [\varphi_2(\omega_l) + \varphi_4(\omega_l)]\,\boldsymbol{V}$

Table 2.1: Matrix form of X in Eq. (2.33) for a neutral and singly charged QD, both for the case without a magnetic field, and with a magnetic field in Faraday and in Voigt configuration. φ_i is the frequency-dependent phase shift (Eq. (2.30)) of the QD transition i. $\boldsymbol{I}$ is the identity matrix, and $\boldsymbol{H}$, $\boldsymbol{V}$, $\boldsymbol{R}$, and $\boldsymbol{L}$ are the Jones polarizer matrices [32].

$$t_1 = \eta_1 \left(1 + 2i\Delta - \frac{2C}{1 - i\Delta'}\right), \tag{2.31}$$

where η_1 is a normalization constant. The advantage of this equation is that the contributions from the empty cavity and QD are separate, which makes it easier to extend to more cavities and QD transitions. In analogy with Eq. (2.31), the single round trip for the case of two cavity modes, and multiple two-level transitions, is described as

$$t_{2x2} = \eta_{2\times2}\left[I_{2\times2} + \begin{pmatrix} 2i\Delta_H & 0 \\ 0 & 2i\Delta_V \end{pmatrix} - R_{-\theta_{QD}} X R_{\theta_{QD}}\right]. \tag{2.32}$$

Now, we can sum over all round trips and find for the total amplitude transmission matrix

$$t_{tot} = \eta_{out}\left[I_{2\times2} - \begin{pmatrix} 2i\Delta_H & 0 \\ 0 & 2i\Delta_V \end{pmatrix} + R_{-\theta_{QD}} X R_{\theta_{QD}}\right]^{-1}. \tag{2.33}$$

We now compare our model to experiments and investigate a neutral QD in a polarization non-degenerate cavity. The device consists of a micropillar cavity with an embedded self-assembled QD [5]. In Fig. 2.3(a), a false color plot of the measured transmission as a function of the relative laser detuning and the orientation of linearly polarized input laser is shown. By careful fitting of our model to the experimental data we obtain excellent agreement (see Fig. 2.3(b)) using the following parameters: $\theta_{QD} = 94° \pm 2°$, cavity splitting $f_V - f_H = 10 \pm 0.1$ GHz, QD fine-structure splitting $f_Y' - f_X' = 2 \pm 0.1$ GHz, $\kappa = 11.1 \pm 0.1$ GHz, $g = 1.59 \pm 0.08$ GHz and $\gamma_\perp = 0.32 \pm 0.15$ GHz (γ^* set to zero). From this, we obtain for both transitions the cooperativity $C = 0.7 \pm 0.5$.

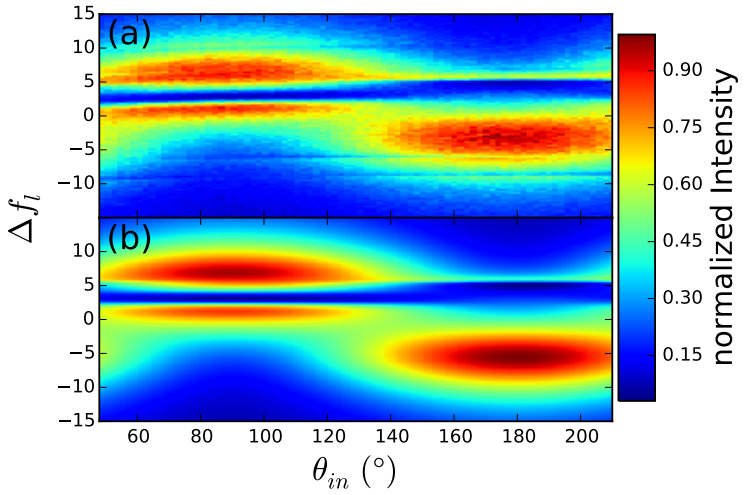

Figure 2.3: False color plot of the cavity transmission as function of laser frequency and linear input polarization orientation. (a) Experimental data, corrected for reduced detection efficiency. (b) Theoretical results based on Eq. (2.33).

2.5 Single photons in the semi-classical model

Now, we show that our model can be used to improve a single photon source based on a neutral QD in a polarization non-degenerate cavity and polarization post-selection. Specifically, we investigate here the single-photon purity (determined by the second-order correlation $g^2(0)$) and the brightness. To calculate $g^2(0)$, we need to take into account two contributions: Firstly, single-photon light that has interacted with the QD $\rho^{sp}(x) = x\,|1\rangle\langle 1| + (1-x)\,|0\rangle\langle 0|$, where x is the mean photon number. Secondly, "leaked" coherent laser light $\rho^{coh}(\alpha)$ with the mean photon number $\left\langle n^{coh}\right\rangle = |\alpha|^2$, where $|\alpha|^2$ can be determined by tuning the QD out of resonance. With a weighting parameter ξ, the density matrix of the total detected light can be written as

$$\rho^{tot} = \left[\xi\rho^{sp}(x) + (1-\xi)\rho^{coh}(\alpha)\right]. \tag{2.34}$$

After determining ρ^{tot}, it is straightforward to obtain $g^{(2)}(0)$ of the total transmitted light [35].

In the next step, we aim to find the optimal polarization condition for using the device as a bright and pure single-photon source. For this, we numerically optimize the input and output polarization, as well as the quantum dot and laser frequency, in order to maximize the light that interacted with the QD transition (single photon light) and to minimize the residual laser light. We compare the optimal result to the trivial polarization conditions 90Cross (excitation of the H- and detection along the V-cavity mode) and 45Circ. For 45Circ, the system is excited with 45° linear polarized light and we detect a single circular polarization component. Fig. 2.4 compares the theoretical prediction to the experimental data for these cases, each with and without the QD. These results show almost perfect agreement between experiment and theory. Only for the 90Cross configuration, the experimental data is slightly higher than expected, which we attribute

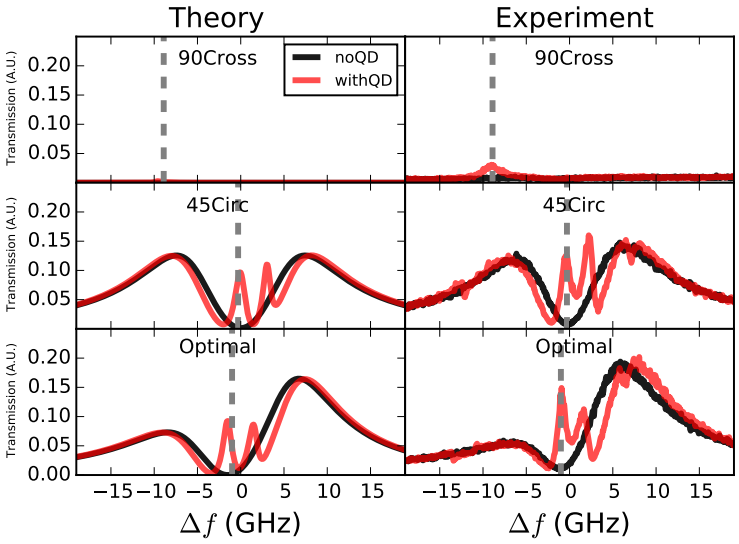

Figure 2.4: Simulated (left) and measured (right) transmitted intensity as a function of the relative laser frequency, with and without the QD and for three polarization configurations: 90Cross (top), 45Circ (center), and Optimal (bottom). For constant laser power, the measured single-photon intensity (frequency indicated by the grey dashed line) of the optimal configuration is about 3× (1.6×) higher compared to the 90Cross (45Circ) configuration.

to small changes of the polarization axes of the QD induced by the necessary electrostatic tuning of the QD resonance.

The optimal polarization condition is found for the input polarization Jones vector $\left(\begin{array}{cc} 0.66, & -0.50 + 0.57i \end{array} \right)^T$ and output polarization $\left(\begin{array}{cc} 0.66, & 0.50 - 0.57i \end{array} \right)^T$. For this case, the single photon intensity is about 3× higher compared to the 90Cross configuration. We emphasize that this optimal configuration can hardly be found experimentally because the parameter space, polarization conditions and QD and laser frequencies, is too large. Instead, numerical optimization has to be done, for which a simple analytical model, like the one presented here, is essential.

For the configurations shown in Fig. 2.4 we now perform power-dependent continuous-wave measurements to determine the experimental brightness and $g^{(2)}(0)$. The laser is locked at the optimal frequency determined by the model (gray-dashed line in Fig. 2.4), and the single photon count rate, as well as the second-order correlation function, is measured using a Hanbury-Brown Twiss setup. The photon count rate is the actual count rate before the first lens, corrected for reduced detection efficiency. Gaussian fits to $g^{(2)}(\tau)$ are used to determine the second-order correlation function at zero time delay $g^{(2)}(0)$.

In Fig. 2.5(a), the single-photon count rate is shown as a function of the input power and in Fig. 2.5(b) we show $g^{(2)}_{exp}(0)$ as a function of the single-photon count rate. In Fig. 2.5(b), we see that, for the optimal configuration, the single photon rate can be up to 24 MHz before the purity of the single-photon source decreases. This means that, for the same purity, it is possible to increase the brightness of the single-photon source

by using different input and output polarization configurations. Note that $g^2_{exp}(0) \approx 0.5$ corresponds to a real $g^{(2)}(0) \approx 0$ due to detector jitter. The two-detector jitter is ≈ 500 ps is of the same order as the cavity enhanced QD decay rate, $1/\left((1+C)\gamma_\perp\right) \sim 300 \pm 150$ ps, which determines the theoretically expected full-width at half maximum of $g^{(2)}(\tau)$ in the case of ideal detectors.

The data in Fig. 2.5(a) shows the interplay between single-photon light scattered from the QD and leaked coherent laser light. We observe a linear slope for high input power, which corresponds to laser light that leaks through the output polarizer. In Fig. 2.5(a) we fit the single photon rate Γ using the formula [4]

$$\left(x + \left\langle n^{coh} \right\rangle\right) \gamma_\perp = \Gamma \frac{\frac{P}{P_0}}{1 + \frac{P}{P_0}} + bP. \tag{2.35}$$

Here, b is the fraction of leaked laser light, P_0 is the saturation power of the QD and Γ the experimentally obtained single photon rate of the QD. We find for the optimal condition $P_0 \approx 3\,\mathrm{nW}$, $\Gamma \approx 40\,\mathrm{MHz}$, and $b \sim 0.5\,\mathrm{MHz\ nW^{-1}}$. This single photon rate is 25 % of the maximal output through one of the mirrors, based on the QD lifetime: $\gamma_\perp/2 \approx 160\,\mathrm{MHz}$.

Calculating $g^{(2)}(0)$ using Eq. (2.34) gives the predictions shown by the dashed lines in Fig. 2.5(b). Here, we used that $\gamma_\perp = 320\,\mathrm{MHz}$ in order to obtain the mean photon numbers. With these mean photon number and considering the detector response, we estimate $\xi_{90} = 0.05$ in Eq. (2.34) for the 90Cross configuration. Changing the value of ξ by the ratios obtained in Fig. 2.4, we obtain the red curve ($\xi_{45} = 1.6 \times \xi_{90} = 0.10$) and blue curve ($\xi_{opt} = 3 \times \xi_{90} = 0.15$), which show that our theory is in good agreement with the experimental data.

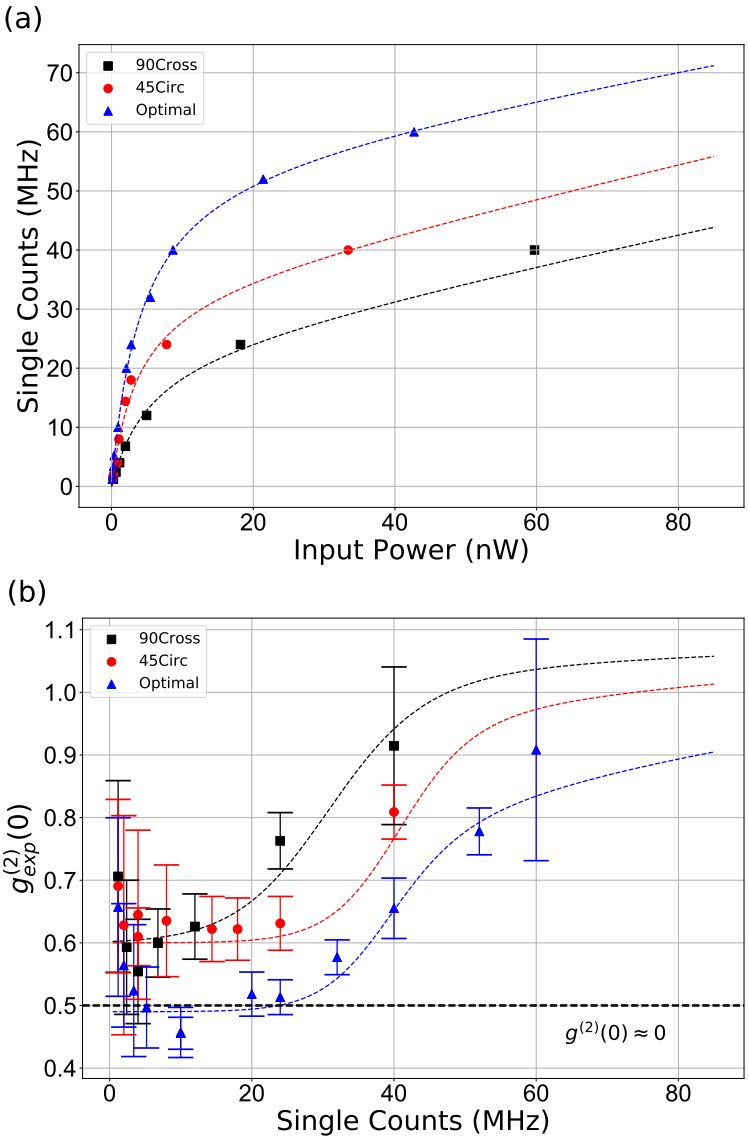

Figure 2.5: (a) Single-photon count rate behind the first lens as a function of the input laser power for the three polarization configurations 90Cross (squares), 45Circ (circles), Optimal (triangles). The dashed lines are fits to Eq. (2.35) and show good agreement. (b) $g^{(2)}_{exp}(0)$ as a function of the measured single-photon count rate behind the first lens. The dashed curves are the theoretical predictions based on the fits in (a). The increased size of the error bars at higher power is because the $g^{(2)}_{exp}(\tau)$ dip becomes small and spectral diffusion appears.

2.6 Conclusion

In principle, if the output polarizer could block all residual laser light, a perfectly pure single-photon source is expected. In this case, the brightness of the single-photon source is determined by the polarization change that the QD-scattered single photons experience. At high power, close to QD saturation, the QD also emits non-resonant light, but its effect on the purity is limited in practice compared to the effect of leaked laser light [36].

In conclusion, we have proposed a polarized semi-classical cavity-QED model and confirmed its accuracy by comparison to experimental data of a QD micro-cavity system. We have shown that this model enables prediction and optimization of the brightness and purity of QD-based single-photon sources, where we have obtained a 3× higher brightness compared to traditional cross-polarization conditions.

2.7 Supplemental material

Derivation of Equation (2.25)

To derive Eq. (2.25) from Eq. (2.24) , we switch to transmission (intensity) instead of the transmission amplitude (electric field). This has the advantage that the imaginary parts disappear and we get a better understanding of each term in the expansion. Using $1-R=t^2=1-r^2$, we obtain from Eq. (2.24)

$$T_{tot}=\frac{(1-R)^2\exp(-2z)}{1+R^2\exp(-4z)-2R\exp(-2z)\cos(-2x_1+\phi)}, \tag{2.36}$$

with $z=a_0+a_{QD}\frac{1}{1+(\Delta')^2}$ and $x_1=a_{QD}\frac{\Delta'}{1+(\Delta')^2}$. Now we use the following approximations: first, we consider small phase changes $\phi\ll 1$. This, in combination with $a_{QD}\ll 1$, allows us to approximate the cosine term as $\cos(-2x_1+\phi)\approx 1-\frac{(-2x_1+\phi)^2}{2}$. Trying to put the equation in a Lorentzian form gives

$$T_{tot}\approx\frac{1}{1+p_0+\left(\frac{-2x_1+\phi}{p_1}\right)^2}, \tag{2.37}$$

with $p_1=\frac{1-R}{\sqrt{R}}$, which corresponds to the finesse of an ideal Fabry-Pérot cavity apart from a factor π. We neglect the x_1^2 in Eq. (2.37) and find

$$T_{tot}\approx\frac{1}{1+p_0+\left(\frac{\phi}{p_1}\right)^2-4\frac{x_1\phi}{p_1^2}}. \tag{2.38}$$

p_0 contains a contribution of loss due to the cavity and the QD. After Taylor expanding p_0 up to second order in z we simplify the analysis by splitting both loss terms and write $p_0=p_c+p_{QD}$ with

$$p_c=2a_0\left(\frac{1+R}{1-R}\right), \tag{2.39}$$

$$p_{QD}=2\frac{1}{1+(\Delta')^2}\left(a_{QD}+a_{QD}^2\right)\left(\frac{1+R}{1-R}\right). \tag{2.40}$$

For the cavity, we take p_c up to first order in a_0 and p_{QD} up to second order in a_{QD}. This choice is made to enable agreement with Eq. 2.27 and will be justified later by comparison to the semi-classical model. With this we can write Eq. (2.38) as

$$T_{tot}\approx\frac{1}{1+p_c}\frac{1}{1+\frac{p_{QD}}{1+p_c}+\frac{\phi^2}{p_1^2(1+p_c)}-4\frac{x_1\phi}{p_1^2(1+p_c)}}. \tag{2.41}$$

With the substitutions

$$\kappa=\frac{2\pi c(1-R)}{nL\sqrt{R}}\sqrt{1+p_c} \tag{2.42}$$

$$\Delta=\frac{f-f_c}{\kappa} \tag{2.43}$$

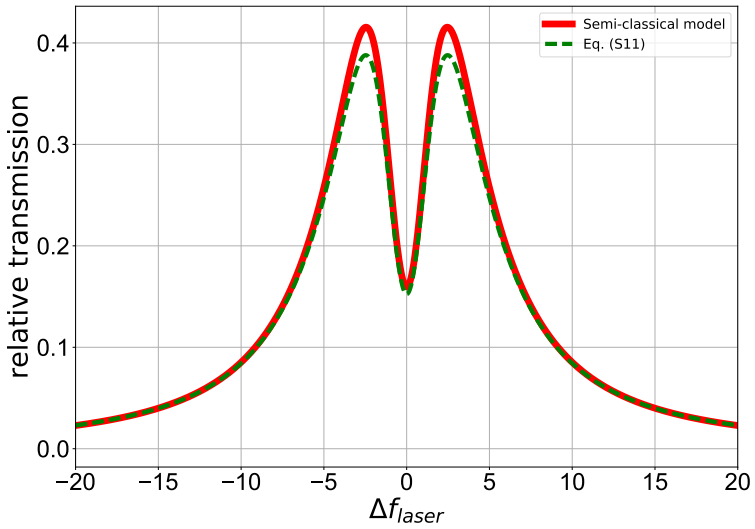

Figure 2.6: Comparison of the semi-classical model of Eq. (2.46) to the exact classical model of the lossy Fabry-Pérot cavity in Eq. (2.36). For low losses and weak coupling, both models agree well.

$$C = a_{QD}\frac{\sqrt{R}}{1-R}\frac{1}{\sqrt{1+p_c}} \tag{2.44}$$

we find for the total transmission

$$T_{tot} \approx \frac{1}{1+p_c}\frac{1}{1+4\Delta^2-8C\frac{\Delta\Delta'}{1+(\Delta')^2}+\frac{2C}{1+(\Delta')^2}(2+2C)}, \tag{2.45}$$

where $\frac{p_{QD}}{1+p_c} \sim \frac{2C}{1+(\Delta')^2}(2+2C)$ assuming that $R \sim 1$. Now we go back to the complex transmission amplitude $t_{tot} = \sqrt{T_{tot}}$ of Eq. (2.45) and find

$$t_{tot} \approx \eta_{out}\frac{1}{1-2i\Delta+\frac{2C}{1-i\Delta'}}. \tag{2.46}$$

In order to confirm that the above approximations are valid we compare Eq. (2.36) to the semi-classical model of Eq. (2.46). In Fig. 2.6, the two models are compared for a cavity with $\lambda = 930\,nm$, $n = 2$, $R = 0.95$, $a_0 = 0.01$, $a_{QD} = 0.03$, and $L = 0.1\,\mu$m. We see that both models agree very well, suggesting that our approximations are valid. The slight deviations in the peak height is due to the assumption that the cavity loss $a_0 \ll 1$ does not completely hold.

Derivation of the semi-classical model in the non-linear regime

In the non-linear regime we do not assume that the QD population is in the ground state, but do allow the operator products to be separated. In this case, for the equations of motion we find

$$\begin{aligned}\langle\dot{a}\rangle &= -\kappa(1-i\Delta_c)\langle\hat{a}\rangle + ig\langle\hat{S}_-\rangle + i\eta,\\ \langle\dot{S}_-\rangle &= -\gamma_\perp(1-i\Delta_Q)\langle\hat{S}_-\rangle + ig\langle\hat{a}\hat{S}_z\rangle,\\ \langle\dot{S}_z\rangle &= -\gamma_{||}(\langle\hat{S}_z\rangle+1) - 2g_0(\langle\hat{a}^\dagger\hat{S}_-\rangle + \langle\hat{S}_+\hat{a}\rangle).\end{aligned} \tag{2.47}$$

Now, making the approximation that the quantum correlations can be neglected leads to

$$\begin{aligned}\langle\dot{a}\rangle &= -\kappa(1-i\Delta_c)\langle\hat{a}\rangle + ig\langle\hat{S}_-\rangle + i\eta,\\ \langle\dot{S}_-\rangle &= -\gamma_\perp(1-i\Delta_Q)\langle\hat{S}_-\rangle + ig\langle\hat{a}\rangle\langle\hat{S}_z\rangle,\\ \langle\dot{S}_z\rangle &= -\gamma_{||}(\langle\hat{S}_z\rangle+1) - 2g_0(\langle\hat{a}^\dagger\rangle\langle\hat{S}_-\rangle + \langle\hat{S}_+\rangle\langle\hat{a}\rangle).\end{aligned} \tag{2.48}$$

There is no formal basis for writing $\langle\hat{a}\hat{S}_z\rangle$ as $\langle\hat{a}\rangle\langle\hat{S}_z\rangle$. The intuition behind it is that for many weakly excited QDs the QD-photon field correlations will tend to zero. In a sense, one might see it as a mean field approximation [20], which holds for many two level transitions. Since it is hard to find the solution of the transmission amplitude as a function of all parameters, we give the solution of the input power as a function of the transmission amplitude. After some math we obtain

$$\frac{\eta}{\kappa} = x\left\{\left(1+\frac{C}{1+\Delta_Q^2+\frac{x^2}{n_0}}\right)^2 + \left(\Delta_c - \frac{C\Delta_Q}{1+\Delta_Q^2+\frac{x^2}{n_0}}\right)^2\right\}^{1/2}, \tag{2.49}$$

where $n_0 = \frac{\gamma_{||}\gamma_\perp}{4g^2}$ is the critical photon number, $x = \langle\hat{a}\rangle$ is the amplitude of the field in the cavity for the transmitted light, C the cooperativity, and Δ_Q and Δ_c are the QD and cavity detunings, respectively. The critical photon number is a measure for the number of photons needed to saturate the response of a single QD. An alternative form of the critical photon number $n_0 = \frac{\gamma_{||}}{C\kappa}$, shows that for increasing cooperativity, less photons are required to saturate the response of the system. Experimentally we observe saturation at a mean photon number of $\langle n\rangle \approx 10^{-2} \equiv n_0$ and use this as an estimate of the critical photon number. The left hand side of Eq. 2.49, given by $\frac{\eta}{\kappa}$, represents the transmission amplitude of the field in an empty cavity on resonance. In Fig. 2.7, we plot the mean photon number of the transmitted light in an empty cavity $\left(\frac{\eta}{\kappa}\right)^2$ versus the mean photon number of the transmitted light in a cavity with QD given by $\langle n\rangle_{cav+QD} = |x|^2$.

At low powers $n_{cav} \ll 1$ we observe that $n_{cav+QD} \approx 0$ which corresponds to the dip in the transmission spectrum for a QD in a cavity (Fig. 2.1), while at very high power we observe the expected linear response, indicating that the effect of the QD is negligible.

In the intermediate region, we find for $C \gtrsim 10$ a bistability in the shape of an S-curve. Coming from a region of low (high) power and slowly increasing (decreasing) to higher power, the mean photon number abruptly jumps to a higher (lower) value, these are called the bistability points (dashed lines in Fig. 2.7). In the experiments reported in this thesis, the maximal cooperativity is $C \approx 3$, therefore we could not investigate this bistability experimentally.

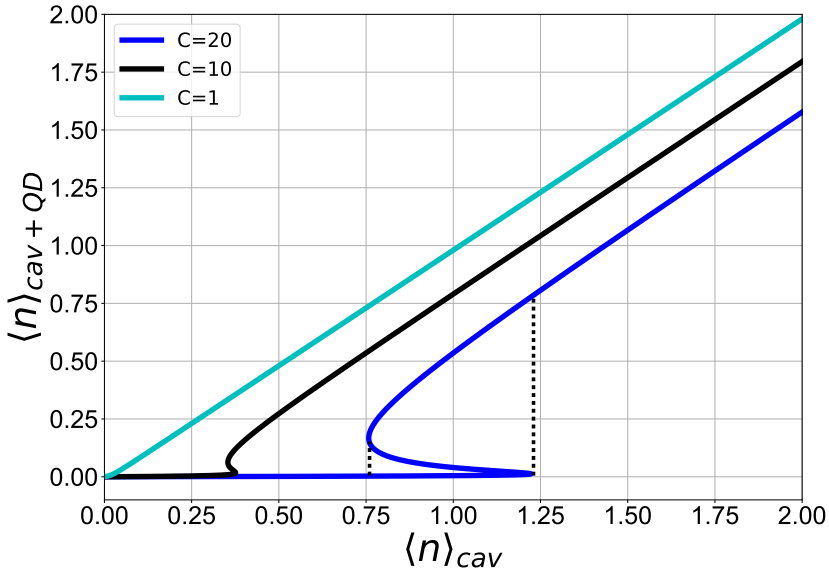

Figure 2.7: Plot of the mean photon number of the transmitted light in an empty cavity versus the mean photon number of the transmitted light in a cavity with QD. The dashed lines indicated the bistability points for QD-cavity system with $C = 20$. Parameters: $\Delta_Q = \Delta_c = 0$ and $n_0 = 10^{-2}$ for all curves.